PHYSICAL REVIEW B **94**, 081116(R) (2016)

Role of $SrTiO_3$ phonon penetrating into thin FeSe films in the enhancement of superconductivity

Shuyuan Zhang,[1] Jiaqi Guan,[1] Xun Jia,[1] Bing Liu,[1] Weihua Wang,[1] Fangsen Li,[2] Lili Wang,[2,3,*] Xucun Ma,[2,3] Qikun Xue,[2,3] Jiandi Zhang,[4] E. W. Plummer,[4] Xuetao Zhu,[1,†] and Jiandong Guo[1,3,‡]

[1]*Beijing National Laboratory for Condensed Matter Physics and Institute of Physics, Chinese Academy of Sciences, Beijing 100190, China*

[2]*State Key Laboratory of Low-Dimensional Quantum Physics, Department of Physics, Tsinghua University, Beijing 100084, China*

[3]*Collaborative Innovation Center of Quantum Matter, Beijing 100871, China*

[4]*Department of Physics and Astronomy, Louisiana State University, Baton Rouge, Louisiana 70808, USA*

(Received 23 May 2016; revised manuscript received 16 August 2016; published 31 August 2016)

The significant role of interfacial coupling in the enhancement of superconductivity in FeSe films on $SrTiO_3$ has been widely recognized, but the explicit origin of this coupling is yet to be identified. Here, by surface phonon measurements using high-resolution electron energy loss spectroscopy, we found the electric field generated by Fuchs-Kliewer (F-K) phonon modes of $SrTiO_3$ can penetrate into FeSe films and strongly interact with the electrons therein. The mode-specific electron-phonon coupling constant for the ~92 meV F-K phonon is ~0.25 in single-layer FeSe on $SrTiO_3$. With increasing FeSe thickness, the penetrating field intensity decays exponentially, which matches well the observed exponential decay of the superconducting gap. It is unambiguously shown that the $SrTiO_3$ F-K phonon penetrating into FeSe is essential for interfacial superconductivity enhancement.

DOI: 10.1103/PhysRevB.94.081116

The recent discovery of high-temperature superconductivity in 1 unit cell (u.c.) FeSe films on a $SrTiO_3$ (STO) substrate [1,2] has attracted a lot of attention, since the superconducting transition temperature (T_C) is significantly raised to ~60–75 K [3–6], even over 100 K [7], from 8 K for the bulk FeSe [8]. Various experiments have been performed to uncover the veiled mechanism of T_C enhancement in this system. Although no explicit conclusion has been reached, two factors are widely believed to be essential—electron doping to FeSe films and the coupling at the interface between FeSe and STO.

The significance of electron doping in interfacial superconductivity enhancement has been evidenced by high-resolution angle-resolved photoemission spectroscopy (ARPES) measurements. Extensive annealing drives electrons transferred from the STO substrate to 1 u.c. FeSe, thus increasing the electron density in the film, and broadening the superconducting gap accordingly [4,9,10]. In fact, superconducting 1 u.c. FeSe/STO has a similar Fermi surface as two other typical electron-doped iron-based superconductors, e.g., $A_xFe_2Se_2$ (A = K,Cs) [11] and (Li,Fe)OHFeSe [12]. The electron density in thick FeSe films can also be tuned by alkali-metal doping [13–16] or by ion-liquid gate tuning [17–19]. Even though the electron density can be raised up to a value as high as that in 1 u. c. FeSe/STO with T_C of 60–75 K, the superconductivity in a thick FeSe film is always weaker (with the highest reported T_C of ~48 K [18]) than that in 1 u.c. FeSe/STO. It is indicated that, besides electron doping, there must be other factor(s) responsible for the enhancement of superconductivity in FeSe/STO.

The importance of interfacial coupling has been directly evidenced by the substrate selection behavior of the enhancement of superconductivity. On oxide substrates such as $SrTiO_3$ or $BiTiO_3$, T_C is strongly enhanced no matter what kinds of crystal orientation, crystal symmetry, or lattice constant the substrates have [20–23], while when thin FeSe films are grown on graphene/SiC(0001) [16,24,25], even though a similar electron density is accomplished by K doping, the maximum superconducting gap is always smaller than that of 1 u.c. FeSe/STO. Moreover, a ferroelectric transition of STO was observed by Raman spectroscopy at ~50 K, quite close to the superconducting T_C of 1 u.c. FeSe/STO, implying a possible correlation between the substrate lattice and enhancement of superconductivity at the interface [26]. Recent high-resolution ARPES measurements show that each energy band of 1 u.c. FeSe is replicated at ~100 meV higher binding energy, which can be attributed to the interaction with the STO optical phonon at around 80 meV [5]. Theoretical analyses further suggested that this strong interaction between the high-energy STO phonon and the electrons in FeSe is responsible for T_C enhancement [5].

All these findings seem to correlate the interfacial coupling with some unique properties of the oxide substrates, especially the optical phonon mode. By measuring the properties directly related to the electronic state, such as the electronic structure or the electron's lifetime, the electron-phonon coupling (EPC) constant can be roughly estimated [5,27], but the involved phonon mode cannot be identified directly, which limits our understanding of the underlying physics. In this Rapid Communication, we report on surface phonon measurements for thin FeSe films grown on STO, obtained by high-resolution electron energy loss spectroscopy (HREELS). From a phonon perspective, our results clearly reveal that the electric field generated by the Fuchs-Kliewer (F-K) [28] surface phonon modes of STO can penetrate into thin FeSe films and strongly interact with the electrons in the FeSe layer with a mode-specific coupling constant value $\lambda_\alpha \sim 0.25$ for the ~92 meV branch. The incomplete screening of the electric field associated with the F-K modes is the key to induce interfacial coupling between FeSe and STO, and further result in an enhancement of superconductivity.

*liliwang@mail.tsinghua.edu.cn
†xtzhu@iphy.ac.cn
‡jdguo@iphy.ac.cn

Thin FeSe films with different thicknesses (1, 2, 3, and 10 u.c.) were grown on a STO (001) surface by molecular beam epitaxy following the procedures reported in Refs. [1,2]. For convenience, these samples will be referred to as 1uc-FeSe/STO, 2uc-FeSe/STO, etc., respectively. All samples were characterized by scanning tunneling microscopy to confirm the high growth quality. The superconducting property of 1uc-FeSe/STO was verified by scanning tunneling spectroscopy and ARPES. The determined superconducting gap (Δ) is around 20 meV and T_C is in the range of 60–70 K. Details about the sample preparation and characterization are given in the Supplemental Material [29].

As a surface-sensitive technique, HREELS is an ideal tool to explore the substrate effects on epitaxial thin films. HREELS measurements, carried out by the recently developed two-dimensional (2D) HREELS system [31], were performed on all samples in the temperature range from 35 to 300 K. Figure 1 shows the HREELS results of 1uc-FeSe/STO at room temperature. Five different energy loss features are observed. The assignments [29] of these features are shown in Table I.

As exhibited in the energy distribution curves (EDCs) of Fig. 1(b), the most prominent features are the α and

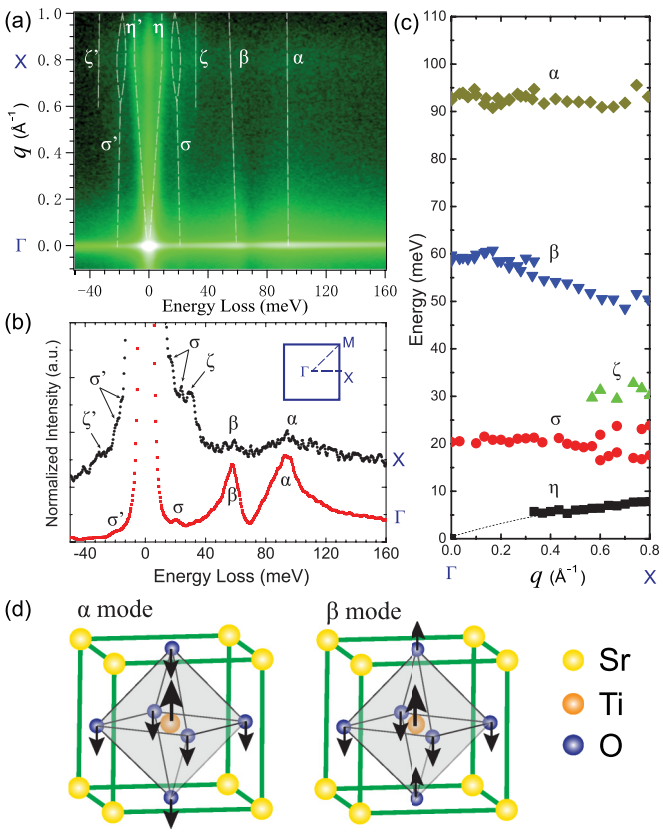

FIG. 1. HREELS results of the 1uc-FeSe/STO sample at room temperature. (a) 2D energy-momentum mapping along the Γ-X direction. Five different phonon modes with positive energy loss are labeled by α, β, σ, ζ, and η, respectively. Dashed lines are provided to guide the eye. The corresponding negative energy loss features correspond to their anti-Stokes peaks, which are labeled by σ',η', etc. (b) EDCs at the Γ point and X point with the inset show the Brillouin zone. (c) Phonon dispersions from the results of (a). (d) Ionic vibrations of the α and β modes [30].

TABLE I. The assignments of the energy loss features.

Feature	Energy ($\hbar\omega$)	Assignment
η	~0–7 meV	Acoustic phonon of FeSe
σ	~20 meV	Optical phonon of FeSe
ζ	~32 meV	Optical phonon of FeSe
β	~60 meV	F-K surface phonon of STO
α	~92 meV	F-K surface phonon of STO

β modes corresponding to the F-K surface phonons of STO [32]. Normally, the phonons of the substrate covered by a metal film should not have been detected by HREELS, but these F-K phonon modes are always accompanied with large dipole oscillations with the electric field extending out of the STO surface [28], as if the F-K modes could penetrate into the epitaxial metal film. In HREELS measurements, the incident electrons are so sensitive to the dipole field [33] that detection of a penetrating electric field from the substrate can be realized. The penetration makes it possible for the electrons in FeSe films to interact with the STO phonons. Moreover, as demonstrated in Fig. 1(c), the energy of the α mode is dispersionless, i.e., almost a constant of ~92 meV within an experimental resolution of about 3 meV at different momentum values, which corroborates the ARPES observation [5] that the replica band is separated from the main band by ~100 meV all throughout the Brillouin zone. Our analysis reveals that this α mode induces rather strong EPCs, and thus in the following we will focus on the α phonon branch as a representative. The contribution of the β mode, with relatively weak EPCs, is described in the Supplemental Material [29].

The HREELS measurements on 1uc FeSe/STO and bare STO are carried out at various temperatures, and the temperature dependence of the energy and linewidth of the α phonon branch are shown in Fig. 2. The phonon energy of bare STO exhibits a very small increase with increasing temperature. In particular, when we take into account an instrument resolution

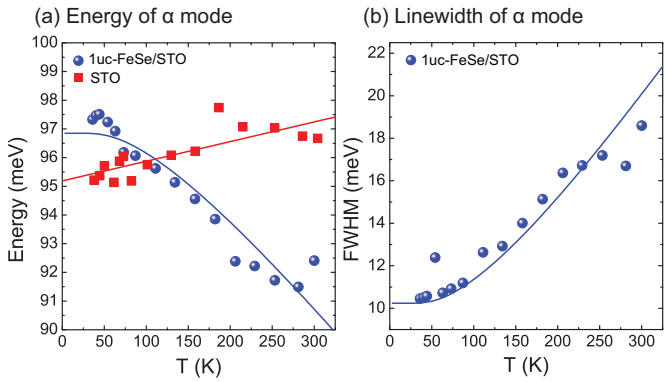

FIG. 2. Temperature dependence of the (a) energy and (b) full width at half maximum (FWHM) of the α phonon branch (blue: 1uc-FeSe/STO; red: bare STO). The dots are experimental data obtained by fitting the EDCs from the HREELS spectra at the Γ point with Gaussian peaks. The red solid line is a linear fitting for bare STO, and the blue solid lines for 1uc-FeSe/STO represent the results of the phonon-phonon decay fitting described in the text.

of about 3 meV, it is negligible. This is consistent with the results in Refs. [34,35]. The linewidth of bare STO is not shown here because it is overlapped with some other collective modes at low temperature and cannot give credible results without a critical analysis. This will be investigated in detail elsewhere. In contrast, the phonon energy as well as the linewidth of 1uc-FeSe/STO show a very strong temperature dependence. Obviously the growth of FeSe on STO drastically changes the energy and its temperature-dependent behavior of the F-K phonon mode. Since F-K phonon modes are strongly related to the dielectric response of STO, the observed T dependence of the F-K mode reflects the coupling between the F-K phonons and the electrons at the interface.

The energy for a specific phonon branch ν at temperature T and momentum $\mathbf{q}$ can be written as a complex form [36],

$$\widetilde{\omega}(\mathbf{q},\nu,T) = \mathrm{Re}[\widetilde{\omega}(\mathbf{q},\nu,T)] - i\,\mathrm{Im}[\widetilde{\omega}(\mathbf{q},\nu,T)], \tag{1}$$

with the energy as the real part,

$$\mathrm{Re}[\widetilde{\omega}(\mathbf{q},\nu,T)] = \omega_0(\mathbf{q},\nu)+\Delta\omega_V(\mathbf{q},\nu;T)+\Delta\omega_{pp}(\mathbf{q},\nu;T), \tag{2}$$

and the linewidth (half width at half maximum) as the imaginary part,

$$\mathrm{Im}[\widetilde{\omega}(\mathbf{q},\nu,T)] = \gamma_{ep}(\mathbf{q},\nu) + \gamma_{pp}(\mathbf{q},\nu;T), \tag{3}$$

where $\omega_0(\mathbf{q},\nu)$ is the harmonic phonon energy at $T = 0$ K including the T-independent EPC contribution, $\Delta\omega_V(\mathbf{q},\nu;T)$ is the energy shift due to the change in the volume, and $\Delta\omega_{pp}(\mathbf{q},\nu;T)$ is the energy shift due to the anharmonic phonon-phonon interactions. The imaginary term $-i\,\mathrm{Im}[\widetilde{\omega}(\mathbf{q},\nu,T)]$ describes the damping of the phonons, with contributions from both EPC $\gamma_{ep}(\mathbf{q},\nu)$ and anharmonicity $\gamma_{pp}(\mathbf{q},\nu;T)$. Considering the anharmonic interaction usually lowers the phonon energy at an elevated temperature, the slight temperature dependence of the α phonon branch of bare STO should be mainly due to a volume change. However, when covered by FeSe, the significant energy decrease with increasing temperature of the α phonon branch should be attributed to a strong anharmonic phonon-phonon interaction.

This anharmonic phonon-phonon interaction can be easily perceived in Table I from the point of view of energy conservation. One can immediately tell that the α mode decaying into the ζ and β modes should be the most favorable decay channel. This conjecture is verified by simulating the anharmonic interaction via three different phonon decay models [29]. Since the α mode is dispersionless (shown in Fig. 1), we set the energy to be $\mathbf{q}$ independent in our models. It turns out the best fitting results are indeed from a model where the α mode with energy $\hbar\omega_0 = 92$ meV decays into two other optical phonon modes (ζ and β) with lower energies $\hbar\omega_1 =$ 60 meV and $\hbar\omega_2 = 32$ meV, where the restriction of energy conservation $\hbar\omega_0 = \hbar\omega_1 + \hbar\omega_2$ is satisfied. In this model, the temperature-dependent phonon energy $\hbar\omega(T)$ and linewidth $\gamma(T)$ are expressed as [37]

$$\hbar\omega(T) = \hbar\omega_a + \hbar\omega_b\left(1 + \frac{1}{e^{\hbar\omega_1/k_BT}-1} + \frac{1}{e^{\hbar\omega_2/k_BT}-1}\right) \tag{4}$$

and

$$\gamma(T) = \gamma_{ep}\left(1 + \frac{1}{e^{\hbar\omega_1/k_BT}-1} + \frac{1}{e^{\hbar\omega_2/k_BT}-1}\right), \tag{5}$$

where $\hbar\omega_a$, $\hbar\omega_b$, and γ_{ep} are fitting parameters. The fitting results are plotted as blue solid lines in Fig. 2. This model explicitly clarifies the large difference in the anharmonic feature between STO and 1uc-FeSe/STO. The 32 meV ζ mode of FeSe, collaborating with the 60 meV β mode of STO, coincidentally renders an appropriate phonon decay channel for the 92 meV α mode. However, if there is no FeSe film, this decay channel is absent in the STO substrate due to the restriction of energy conservation. Hence this anharmonic interaction characterizes part of the interfacial coupling. Its role in the enhancement of superconductivity is not yet clear. Further studies are needed to figure out the explicit role of the anharmonicity.

The other part of the interfacial coupling, the penetrating STO F-K phonons interacting with the electrons in FeSe, is directly relevant to the enhancement of superconductivity. The strength of this interaction can be characterized by a mode-specific EPC constant $\lambda(\mathbf{q},\nu)$ for a single phonon mode of wave vector $\mathbf{q}$ and branch ν, which is related to the EPC-induced linewidth $\gamma_{ep}(\mathbf{q},\nu)$ by Allen's formula [38,39],

$$\lambda(\mathbf{q},\nu) = \frac{2\gamma_{ep}(\mathbf{q},\nu)}{\pi N(E_F)\hbar^2\omega^2(\mathbf{q},\nu)}, \tag{6}$$

where $\omega(\mathbf{q},\nu)$ is the phonon frequency and $N(E_F)$ is the density of states for both spins in each unit cell at the Fermi energy.

To obtain the EPC constant from Allen's formula, the EPC-induced linewidth $\gamma_{ep}(\mathbf{q},\nu)$ should be a prerequisite quantity. However, it is challenging to directly obtain pure EPC-induced phonon linewidths from experiment, because the measured phonon linewidths also contain additional contributions from anharmornic phonon-phonon interactions, as shown in Eq. (3). Only when the temperature-dependent anharmonic phonon-phonon interaction is correctly deducted, can the EPC-induced linewidth γ_{ep} be determined and λ be calculated. This can be accomplished from measurements of the temperature dependence of the phonon dispersions [36] (see Fig. 2). We extract γ_{ep} for the α mode through the above anharmonic phonon decay model, as shown in Eqs. (4) and (5), which gives $\gamma_{ep}(\alpha) = \gamma(T = 0) \cong 5.1$ meV, since there is no phonon-phonon interaction at $T = 0$ and $\gamma(T = 0)$ is the linewidth with EPC only. Independently, by analyzing the temperature dependence of the phonon energy, we have also tried another approach using the Kramers-Kronig relation to obtain $\gamma_{ep}(\alpha)$ [29]. In this method, $\gamma_{pp}(\nu;T)$ in Eq. (3) can be estimated through the Kramers-Kronig transformation of $\Delta\omega_{pp}(\nu;T)$ in Eq. (2), which can be determined from a fitting of experimental data. Hence, by subtracting the anharmonic contribution $\gamma_{pp}(\alpha;T)$ from the measured linewidth $\gamma(\alpha;T)$, we obtained $\gamma_{ep}(\alpha) \cong 4.5$ meV [29].

On the other hand, a simple tight-binding model is applied to fit the electron band structure near the Fermi surface to calculate the density of states $N(E_F) = 1.4\times10^{-3}$ $(\mathrm{meV})^{-1}$ [29]. Thus the EPC constant of the α mode could be obtained from Eq. (6), $\lambda_\alpha \sim 0.25$. This coupling constant is significant for such a high-energy phonon mode, which plays a major

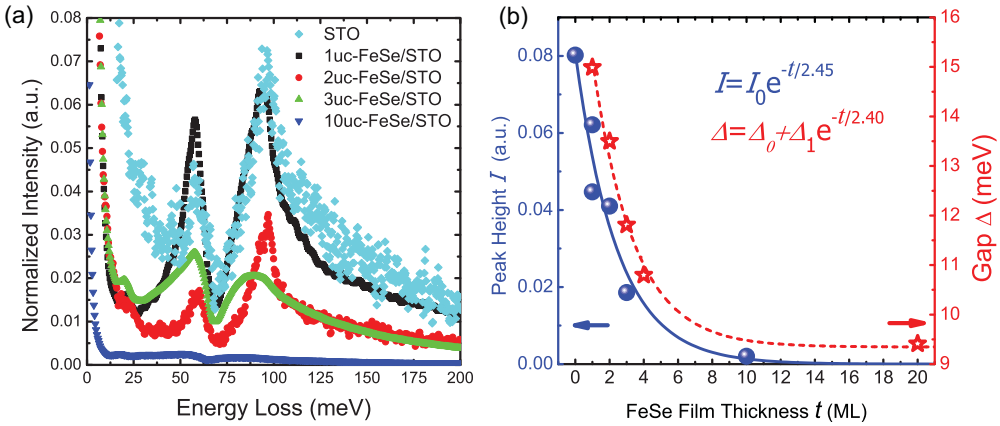

FIG. 3. (a) EDCs at the Γ point for samples with different FeSe thicknesses. (b) Plot and exponential fitting of the peak height of the α mode as a function of the FeSe thickness (blue). Plot and exponential fitting of the superconducting gap size for the K-doped FeSe/STO as a function of the FeSe thickness (red), with data extracted from Ref. [25].

role in the enhancement of superconductivity [40]. The same analysis is performed for the β mode and gives $\lambda_\beta \sim 0.1$. These EPC constants are mainly attributed to the interactions with electrons in FeSe films, since the electron density in STO is much lower than FeSe after electron transfer [6]. The sum of the two EPC constants is $\lambda_{\alpha+\beta} \sim 0.35$, which dominantly accounts for the calculated total EPC constant of about 0.4 from the STO substrate [41]. The higher-energy α mode has a stronger interaction than the β mode, as evidenced from previous ARPES results that the 100 meV replica band is much clearer than the 60 meV replica band [5]. This can also be understood by the fact that the α mode generates a stronger dipole field than the β mode. As shown in Fig. 1(d), all six oxygen ions vibrate in the opposite direction with the titanium ions in the α mode, while the two apical oxygen ions vibrate in the same direction with the titanium ions in the β mode [30].

The above results give direct evidence that the electric field generated by the F-K phonon modes of STO can penetrate the FeSe films and strongly interact with the electrons in the FeSe layer. But how far can this electric field penetrate? To answer this question, we performed HREELS measurements on samples with different FeSe thicknesses (2, 3, and 10 u.c.) to study the spatial spreading properties of the F-K modes. In Fig. 3(a) we plot the normalized EDCs at the Γ point for the samples with different FeSe thicknesses, which apparently demonstrates the decay of the α and β modes with increasing FeSe thickness. An exponential fit to the normalized peak height of the α mode [blue dots in Fig. 3(b)] gives a decay length of 2.5 u.c., which can be regarded as a characteristic length of F-K mode penetration in FeSe films. A recent study of the thickness-dependent superconducting gaps of K-doped FeSe films presents very similar behavior, i.e., the gap size decreases exponentially with increasing FeSe thickness characterized by a decay length of 2.40 u.c. [red stars in Fig. 3(b)] [25]. Considering the similar carrier densities at the interfacial layer [42], the striking coincidence between the two characteristic lengths suggests that the α phonon of STO is closely related to the enhancement of superconductivity at the FeSe/STO interface. The electrons in FeSe spontaneously screen the F-K electric field and lead to the decay of the field intensity, which weakens the enhancement of superconductivity. This is why the superconducting gap can only be enhanced within 3 u.c. FeSe films [43,44].

The screening length to an external electric field by a metal is inversely proportional to the electron density of the metal [45]. Raising the electron-doping level of the FeSe film, although helpful to increase the superfluid density, will inhibit the penetration length of the dipole field from STO. Therefore, there is always a trade-off between the electron density and the field penetration. This is possibly the cause of a gap decrease when extra electrons are doped in 1uc-FeSe/STO [43]. As a result, increasing the doping level in FeSe may not be able to further enhance the superconductivity if the dipole field from the substrate is not penetrating effectively into the FeSe films. Searching for substrates with F-K phonons that generate a strong dipole field is a feasible route.

In conclusion, our HREELS study provides a microscopic understanding of the enhancement of superconductivity in the FeSe/STO system. First, we determine the origin of the interfacial coupling. It is the F-K phonon modes in STO, generating a long-range dipole field, that strongly interact with the electrons in the FeSe layer. The mode-specific EPC constant is ~0.25 for the ~92 meV phonon in 1uc FeSe/STO. This interaction is closely related to the enhancement of superconductivity. Second, we determine the characteristic penetration depth of the STO F-K phonon into the FeSe film. The decay of the penetrating phonon results in the thickness limit of the enhancement of superconductivity in FeSe/STO. Therefore, ionic crystals with high-energy F-K phonon modes that generate a strong dipole field, for instance, oxides with high valence metal ions and long oxygen-metal bonds, should be good candidates for the substrates.

X.Z. acknowledges helpful discussions with Professor M. El-Batanouny, and thanks Dr. Yan Wang for pointing out the initial error in calculating the EPC constant. This work is supported by NSFC (Grants No. 11225422 and No. 11304367), MOSTC (Grants No. 2012CB921700 and No. 2015CB921000), the Strategic Priority Research Program (B) of CAS (Grant No. XDB07010100), and the External Cooperation Program of BIC, CAS (Grant No. 112111KYSB20130007).

[1] Q.-Y. Wang, Z. Li, W.-H. Zhang, Z.-C. Zhang, J.-S. Zhang, W. Li, H. Ding, Y.-B. Ou, P. Deng, K. Chang, J. Wen, C.-L. Song, K. He, J.-F. Jia, S.-H. Ji, Y.-Y. Wang, L.-L. Wang, X. Chen, X.-C. Ma, and Q.-K. Xue, Chin. Phys. Lett. **29**, 037402 (2012).

[2] W.-H. Zhang, Y. Sun, J.-S. Zhang, F.-S. Li, M.-H. Guo, Y.-F. Zhao, H.-M. Zhang, J.-P. Peng, Y. Xing, H.-C. Wang, T. Fujita, A. Hirata, Z. Li, H. Ding, C.-J. Tang, M. Wang, Q.-Y. Wang, K. He, S.-H. Ji, X. Chen, J.-F. Wang, Z.-C. Xia, L. Li, Y.-Y. Wang, J. Wang, L.-L. Wang, M.-W. Chen, Q.-K. Xue, and X.-C. Ma, Chin. Phys. Lett. **31**, 017401 (2014).

[3] W. Zhang, Z. Li, F. Li, H. Zhang, J. Peng, C. Tang, Q. Wang, K. He, X. Chen, L. Wang, X. Ma, and Q.-K. Xue, Phys. Rev. B **89**, 060506 (2014).

[4] D. Liu, W. Zhang, D. Mou, J. He, Y.-B. Ou, Q.-Y. Wang, Z. Li, L. Wang, L. Zhao, S. He *et al.*, Nat. Commun. **3**, 931 (2012).

[5] J. Lee, F. Schmitt, R. Moore, S. Johnston, Y.-T. Cui, W. Li, M. Yi, Z. Liu, M. Hashimoto, Y. Zhang *et al.*, Nature (London) **515**, 245 (2014).

[6] S. Tan, Y. Zhang, M. Xia, Z. Ye, F. Chen, X. Xie, R. Peng, D. Xu, Q. Fan, H. Xu *et al.*, Nat. Mater. **12**, 634 (2013).

[7] J.-F. Ge, Z.-L. Liu, C. Liu, C.-L. Gao, D. Qian, Q.-K. Xue, Y. Liu, and J.-F. Jia, Nat. Mater. **14**, 285 (2015).

[8] F.-C. Hsu, J.-Y. Luo, K.-W. Yeh, T.-K. Chen, T.-W. Huang, P. M. Wu, Y.-C. Lee, Y.-L. Huang, Y.-Y. Chu, D.-C. Yan *et al.*, Proc. Natl. Acad. Sci. USA **105**, 14262 (2008).

[9] S. He, J. He, W. Zhang, L. Zhao, D. Liu, X. Liu, D. Mou, Y.-B. Ou, Q.-Y. Wang, Z. Li *et al.*, Nat. Mater. **12**, 605 (2013).

[10] J. He, X. Liu, W. Zhang, L. Zhao, D. Liu, S. He, D. Mou, F. Li, C. Tang, Z. Li *et al.*, Proc. Natl. Acad. Sci. USA **111**, 18501 (2014).

[11] Y. Zhang, L. Yang, M. Xu, Z. Ye, F. Chen, C. He, H. Xu, J. Jiang, B. Xie, J. Ying *et al.*, Nat. Mater. **10**, 273 (2011).

[12] L. Zhao, A. Liang, D. Yuan, Y. Hu, D. Liu, J. Huang, S. He, B. Shen, Y. Xu, X. Liu, L. Yu, G. Liu, H. Zhou, Y. Huang, X. Dong, F. Zhou, K. Liu, Z. Lu, Z. Zhao, C. Chen, Z. Xu, and X. J. Zhou, Nat. Commun. **7**, 10608 (2016).

[13] J. Seo, B. Kim, B. Kim, J. Jeong, J. Ok, J. S. Kim, J. Denlinger, S.-K. Mo, C. Kim, and Y. Kim, Nat. Commun. **7**, 11116 (2016).

[14] C. Wen, H. Xu, C. Chen, Z. Huang, X. Lou, Y. Pu, Q. Song, B. Xie, M. Abdel-Hafiez, D. Chareev *et al.*, Nat. Commun. **7**, 10840 (2016).

[15] Y. Miyata, K. Nakayama, K. Sugawara, T. Sato, and T. Takahashi, Nat. Mater. **14**, 775 (2015).

[16] C.-L. Song, H.-M. Zhang, Y. Zhong, X.-P. Hu, S.-H. Ji, L. Wang, K. He, X.-C. Ma, and Q.-K. Xue, Phys. Rev. Lett. **116**, 157001 (2016).

[17] J. Shiogai, Y. Ito, T. Mitsuhashi, T. Nojima, and A. Tsukazaki, Nat. Phys. **12**, 42 (2016).

[18] B. Lei, J. H. Cui, Z. J. Xiang, C. Shang, N. Z. Wang, G. J. Ye, X. G. Luo, T. Wu, Z. Sun, and X. H. Chen, Phys. Rev. Lett. **116**, 077002 (2016).

[19] K. Hanzawa, H. Sato, H. Hiramatsu, T. Kamiya, and H. Hosono, Proc. Natl. Acad. Sci. USA **113**, 3986 (2016).

[20] R. Peng, X. P. Shen, X. Xie, H. C. Xu, S. Y. Tan, M. Xia, T. Zhang, H. Y. Cao, X. G. Gong, J. P. Hu, B. P. Xie, and D. L. Feng, Phys. Rev. Lett. **112**, 107001 (2014).

[21] R. Peng, H. Xu, S. Tan, H. Cao, M. Xia, X. Shen, Z. Huang, C. Wen, Q. Song, T. Zhang *et al.*, Nat. Commun. **5**, 5044 (2014).

[22] P. Zhang, X.-L. Peng, T. Qian, P. Richard, X. Shi, J.-Z. Ma, B.-B. Fu, Y.-L. Guo, Z. Han, S. Wang *et al.*, arXiv:1512.01949.

[23] G. Zhou, D. Zhang, C. Liu, C. Tang, X. Wang, Z. Li, C. Song, S. Ji, K. He, L. Wang, X. Ma, and Q.-K. Xue, Appl. Phys. Lett. **108**, 202603 (2016).

[24] C.-L. Song, Y.-L. Wang, P. Cheng, Y.-P. Jiang, W. Li, T. Zhang, Z. Li, K. He, L. Wang, J.-F. Jia, H.-H. Hung, C. Wu, X. Ma, X. Chen, and Q.-K. Xue, Science **332**, 1410 (2011).

[25] W. H. Zhang, X. Liu, C. H. P. Wen, R. Peng, S. Y. Tan, B. P. Xie, T. Zhang, and D. L. Feng, Nano Lett. **16**, 1969 (2016).

[26] Y.-T. Cui, R. G. Moore, A.-M. Zhang, Y. Tian, J. J. Lee, F. T. Schmitt, W.-H. Zhang, W. Li, M. Yi, Z.-K. Liu, M. Hashimoto, Y. Zhang, D.-H. Lu, T. P. Devereaux, L.-L. Wang, X.-C. Ma, Q.-M. Zhang, Q.-K. Xue, D.-H. Lee, and Z.-X. Shen, Phys. Rev. Lett. **114**, 037002 (2015).

[27] Y. C. Tian, W. H. Zhang, F. S. Li, Y. L. Wu, Q. Wu, F. Sun, G. Y. Zhou, L. Wang, X. Ma, Q.-K. Xue, and J. Zhao, Phys. Rev. Lett. **116**, 107001 (2016).

[28] R. Fuchs and K. L. Kliewer, Phys. Rev. **140**, A2076 (1965).

[29] See Supplemental Material at http://link.aps.org/supplemental/10.1103/PhysRevB.94.081116 for details.

[30] H. Vogt, Phys. Rev. B **38**, 5699 (1988).

[31] X. Zhu, Y. Cao, S. Zhang, X. Jia, Q. Guo, F. Yang, L. Zhu, J. Zhang, E. Plummer, and J. Guo, Rev. Sci. Instrum. **86**, 083902 (2015).

[32] A. D. Baden, P. A. Cox, R. G. Egdell, A. F. Orchard, and R. J. D. Willmer, J. Phys. C **14**, L1081 (1981).

[33] H. Ibach and D. L. Mills, *Electron Energy Loss Spectroscopy and Surface Vibrations* (Academic Press, New York, 1982).

[34] J. L. Servoin, Y. Luspin, and F. Gervais, Phys. Rev. B **22**, 5501 (1980).

[35] C. Perry, J. H. Fertel, and T. McNelly, J. Chem. Phys. **47**, 1619 (1967).

[36] G. Grimvall, *The Electron-Phonon Interaction in Metals*, Vol. 8 (North-Holland, Amsterdam, 1981).

[37] J. Menéndez and M. Cardona, Phys. Rev. B **29**, 2051 (1984).

[38] P. B. Allen, Solid State Commun. **14**, 937 (1974).

[39] P. Allen, in *Dynamical Properties of Solids*, edited by G. K. Horton and A. A. Maradudin (North-Holland, Amsterdam, 1980), Vol. 3, p. 95.

[40] Y. Wang, A. Linscheid, T. Berlijn, and S. Johnston, Phys. Rev. B **93**, 134513 (2016).

[41] Y. Zhou and A. J. Millis, Phys. Rev. B **93**, 224506 (2016).

[42] Z. R. Ye, C. F. Zhang, H. L. Ning, W. Li, L. Chen, T. Jia, M. Hashimoto, D. H. Lu, Z.-X. Shen, and Y. Zhang, arXiv:1512.02526.

[43] C. Tang, D. Zhang, Y. Zang, C. Liu, G. Zhou, Z. Li, C. Zheng, X. Hu, C. Song, S. Ji, K. He, X. Chen, L. Wang, X. Ma, and Q.-K. Xue, Phys. Rev. B **92**, 180507 (2015).

[44] C. Tang, C. Liu, G. Zhou, F. Li, H. Ding, Z. Li, D. Zhang, Z. Li, C. Song, S. Ji, K. He, L. Wang, X. Ma, and Q.-K. Xue, Phys. Rev. B **93**, 020507 (2016).

[45] A. K. Theophilou, J. Phys. F **2**, 1124 (1972).